International Journal of Neural Systems, Vol. 25, No. 3 (2015) 1550007 (23 pages)

DOI: 10.1142/S0129065715500070

Discrimination of Schizophrenia Auditory Hallucinators by Machine Learning of Resting-State Functional MRI

Darya Chyzhyk* and Manuel Graña
Computational Intelligence Group
Universidad del Pais Vasco (UPV/EHU)
San Sebastian 20018, Spain
**darya.chyzhyk@ehu.es*

Döst Öngür and Ann K. Shinn
McLean Hospital, Belmont, MA, USA
Harvard Medical School, Boston, MA, USA

Accepted 14 January 2015
Published Online 10 March 2015

Auditory hallucinations (AH) are a symptom that is most often associated with schizophrenia, but patients with other neuropsychiatric conditions, and even a small percentage of healthy individuals, may also experience AH. Elucidating the neural mechanisms underlying AH in schizophrenia may offer insight into the pathophysiology associated with AH more broadly across multiple neuropsychiatric disease conditions. In this paper, we address the problem of classifying schizophrenia patients with and without a history of AH, and healthy control (HC) subjects. To this end, we performed feature extraction from resting state functional magnetic resonance imaging (rsfMRI) data and applied machine learning classifiers, testing two kinds of neuroimaging features: (a) functional connectivity (FC) measures computed by lattice auto-associative memories (LAAM), and (b) local activity (LA) measures, including regional homogeneity (ReHo) and fractional amplitude of low frequency fluctuations (fALFF). We show that it is possible to perform classification within each pair of subject groups with high accuracy. Discrimination between patients with and without lifetime AH was highest, while discrimination between schizophrenia patients and HC participants was worst, suggesting that classification according to the symptom dimension of AH may be more valid than discrimination on the basis of traditional diagnostic categories. FC measures seeded in right Heschl's gyrus (RHG) consistently showed stronger discriminative power than those seeded in left Heschl's gyrus (LHG), a finding that appears to support AH models focusing on right hemisphere abnormalities. The cortical brain localizations derived from the features with strong classification performance are consistent with proposed AH models, and include left inferior frontal gyrus (IFG), parahippocampal gyri, the cingulate cortex, as well as several temporal and prefrontal cortical brain regions. Overall, the observed findings suggest that computational intelligence approaches can provide robust tools for uncovering subtleties in complex neuroimaging data, and have the potential to advance the search for more neuroscience-based criteria for classifying mental illness in psychiatry research.

Keywords: Resting state fMRI; Schizophrenia; machine learning; feature selection; lattice computing; functional connectivity; lattice auto-associative memories.

1. Introduction

Auditory hallucinations (AH) are auditory perceptions in the absence of external acoustical stimuli.[3,59] They are a common symptom in schizophrenia, but they can be present in other psychiatric disorders, in neurological conditions, such as epilepsy,[33] in states of drug intoxication or withdrawal, and even in 10–15% of healthy subjects.[85,89] The pathophysiology

underlying AH may be shared to some degree across multiple disease conditions. Thus, elucidating the neural mechanisms underlying AH in schizophrenia may offer insight into the mechanisms associated with AH more broadly.

Several models of AH pathogenesis have been proposed,[3,36,40,59,63,65,71,83,95] but the exact pathophysiology remains unclear. According to inner speech theories, AH occur when inner speech is misattributed as originating outside the self. Source monitoring accounts focus on preconscious top-down cognitive processes such as the influence of cues, personal beliefs, and expectations in the failure to recognize "self" attributes of inner speech.[17,41,91] Feed forward models, which provide a more bottom-up explanatory framework, propose that AH result from a breakdown in corollary discharge, a system that signals via an "efference copy" that a particular motor output is about to be produced.[20,21] In the case of inner speech, discharges from motor speech production areas fail to inhibit speech perception areas, and the self-produced speech is thus perceived as coming from an external source.[23] Studies investigating such feed forward models tend to focus on structural and functional disconnection between the frontal and temporo-parietal areas.[3,59,81,84] Models based in signal detection theory[5] suggest that AH result from greater perceptual bias to detect auditory signals, especially signals consisting of personally salient words.[18] A memory-based model proposes that AH are unintentionally activated auditory representations from memory which have been dissociated from their original context.[94] A more neuroanatomically oriented model proposes that AH arise from heightened bottom-up activity in the left superior temporal gyrus (STG) priming the brain for "over-perceptualization", combined with a failure of top-down control from the anterior cingulate, prefrontal, premotor, and cerebellar cortices leading to a breakdown in monitoring.[3] A similar model suggests it is the failure of prefrontal executive functions to inhibit activity in the STG (the perceptual origin of AH) and parietal cortex (the purported center of attention to the voice), due to frontotemporoparietal disconnection, that leads to AH.[36] Still another hypothesis, focusing on network connectivity,[64] suggests that abnormal interaction between the default mode network and the auditory cortex at rest is the fundamental mechanism leading to AH. Most of these models are not mutually exclusive, and there are ongoing efforts to integrate such models into a more unified view.[95]

Studies on the neural substrates associated with AH pathophysiology, as proposed in the above and other AH models, have utilized a wide range of neuroimaging techniques.[3] These include volumetric and morphometric magnetic resonance imaging (MRI) studies,[48,71] diffusion tensor imaging (DTI) to assess white matter integrity,[14] functional activation studies using positron emission tomography (PET) or functional MRI (fMRI),[86] and functional connectivity (FC) studies[16,40,51,52] using resting-state fMRI (rsfMRI).[24,76] rsfMRI enables the study of correlations between low frequency components of voxel time series,[7] which are proposed to reflect intrinsic functional correlations between brain regions.[7,101] rsfMRI data are aquired in awake subjects in a passive mind state; because rsfMRI does not impose on the cognitive abilities of the subjects, it can be performed with a wide variety of subjects and cognitive conditions. rsfMRI has been used to study brain development,[19] depression,[31,100] Alzheimer's Disease,[55] and schizophrenia.[61,70,96,105,106]

rsfMRI studies of schizophrenia patients with AH have used varying methods and asked different questions about AH-related connectivity.[11,25,34,54,68,80,81,84,92,97] A recent study by members of our group[81] investigated differences between schizophrenia patients with and without a history of AH in the resting state network correlating with voxels in left Heschl's gyrus (LHG) (Montreal Neurological Institute (MNI) coordinates −42, −26, 10), the location of the primary auditory cortex in humans.[13] The LHG seed was selected because it has been identified in anatomical[62,71] and functional studies[16] as important in AH pathogenesis. We found that LHG FC to classical Broca's territory in inferior frontal gyrus (IFG), dorsal anterior cingulate cortex (dACC), and other frontotemporal regions is elevated in AH and covaries with AH severity. In contrast to the results from the symptom covariate analysis, the findings from the group-wise comparisons were less robust.

Machine learning,[2,82] which is a branch of artificial intelligence, provides new ways to analyze neuroimaging data[50,102] and may offer advantages over traditional statistical inference approaches (for details, see Sec. 3.1 describing the rationale for the

approach). In machine learning models, dependent variables can be predicted on the basis of features extracted from the data. The feature extraction process, involving voxel saliency measures, can provide imaging biomarkers for the phenomena under study when the discriminant values can be mapped onto anatomical locations. Classification performance, as measured by accuracy and other indices, then enables assessment of a model's predictive power. A variety of computational intelligence approaches have previously been applied to rsfMRI data analysis. These include artificial neural networks,[57] multivariate pattern analysis (MVPA),[19,72] and a spiking neural network.[98]

In this paper, we apply a novel lattice computing-based machine learning approach[27,29,30] to measure the accuracy with which rsfMRI data from schizophrenia patients with a history of AH (SZAH) can be discriminated from that of schizophrenia patients without a history of AH (SZNAH) and healthy controls (HC). In mathematics, a lattice is a partially ordered set in which every set of two elements has a *join* (or least upper bound) and a *meet* (or greatest lower bound).[6] Inspired by mathematical morphology, lattice computing[29,44,45] provides a nonlinear approach to computational problem solving. In general terms, algorithms are built on lattice algebra $[(\mathbb{R}^n, \wedge, \vee, +)$ where $\wedge$ and $\vee$ are the minimum and maximum binary operators], instead of conventional linear algebra $(\mathbb{R}^n, +, \times)$.[78] Lattice computing provides numerically robust solutions, avoiding the problem of inverse computations which are inherent in linear approaches. Lattice computing is also faster than linear approaches because multiplications are replaced by additions in the construction of algorithms.

Auto-associative memories are intended to store patterns and to retrieve them from noisy or missing data. *Linear* auto-associative memories are single-layer networks made of interconnected linear units that operate in parallel.[47] Because the representation of individual stimuli is not localized in the memory but distributed throughout the entire network, an auto-associative memory is able to retrieve an entire pattern of information given only partial or degraded versions of these stimuli; because of this property, auto-associative memories are often used in pattern recognition algorithms and for modeling human perceptual learning and memory.[1] *Lattice* auto-associative memories (LAAMs)[77,79] are built by replacing the linear algebraic functions of linear auto-associative memories with those of lattice algebra. In algorithms using auto-associative memories, recall error is the distance between the expected and actual recall patterns. With LAAM's, the distance between the recalled input and the actual input may be used as a nonlinear measure of similarity, which may be used as an alternative to correlation measures in FC analysis. LAAM's show perfect recall of vectors whose elements are real numbers. In addition, because LAAM's can recover stored patterns from even heavily distorted information, they are robust to specific types of noise. Because of this latter property, the distance between the recalled input and the actual input may be used as a nonlinear measure of similarity, which may be used as an alternative to correlation measures in FC analysis. While methods involving LAAM-based distance cannot be expected to reproduce exactly the findings of methods using Pearson's correlation coefficient, the LAAM findings may provide a complementary view of the data.

Besides LAAM-based FC, there are other features that can be extracted from rsfMRI data. Local activity (LA) measures include regional homogeneity (ReHo), which measures the correlation between the fMRI time series of a voxel and that of neighboring voxels[104]; and the amplitude of low frequency fluctuations (ALFF) and fractional amplitude of low frequency fluctuations (fALFF),[107] which measure the strength of low frequency oscillations (LFOs) of the fMRI time series. ReHo and fALFF provide information about regional homogeneity and activation magnitude, respectively, and can offer insights that are complementary to information about FC.

Here, using LAAM-based FC to assess LHG connectivity with spatially distributed brain regions, and ReHo and fALFF to assess LA, we demonstrate high accuracy, sensitivity, and specificity in discriminating SZAH from SZNAH and HC. To our knowledge, this is the first study to apply machine learning techniques, especially a novel lattice-based FC algorithm, to the classification of schizophrenia patients with and without AH.

2. Materials

We performed computational experiments on rsfMRI data from 68 men and women, aged 18–65 years,

divided in three groups: (i) 26 schizophrenia patients (14 schizophrenia, 12 schizoaffective disorder, 1 schizophreniform disorder) with a history of AH (SZAH), (ii) 14 schizophrenia patients (5 schizophrenia, 8 schizoaffective disorder, and 1 schizophreniform disorder) without a history of AH (SZNAH), and (iii) 28 HC subjects. Data from one SZAH subject in the original dataset did not meet the current experiment's criteria for angular head motion less than 3° and were thus not included. The Structured Clinical Interview for DSM-IV-TR (SCID)[22] was administered to confirm axis I diagnosis in patients and to rule out major psychiatric illness in HC subjects. Item B16 of the SCID ("Did you ever hear things that other people could not, such as noises, or the voices of people whispering or talking?") was used to categorize patients into the SZAH and SZNAH groups; patients scoring threshold/true on B16 were coded SZAH, and all others SZNAH. AH severity was assessed with the psychotic symptom rating scale, AH subscale (PSYRATS-AH).[32] Subjects were additionally interviewed post-scan about the presence of AH during image acquisition. PSYRATS-AH and post-scan debriefing interviews were not completed in $n = 7$ SZNAH patients whose data were acquired as part of a different dataset. Nearly all ($n = 24/26$) SZAH patients experienced verbal AH, as confirmed during the research interview and/or documented in the patients' medical records; verbal AH could not be confirmed in two SZAH patients whose imaging data were originally acquired as part of a different dataset. For each subject we acquired 240 blood oxygen level dependent (BOLD) volumes and one T1-weighted anatomical image. Detailed participant characteristics (e.g. age, gender, handedness, illness duration, medication profiles) and image acquisition parameters are provided in the previous paper.[81]

3. Methods

Our machine learning pipeline involved multiple steps, which are summarized in Fig. 1 for the specific lattice computing-based feature extraction approach. Briefly, they are: (1) Preprocessing. (2) Dimensionality reduction, which involved mapping the multivariate information (BOLD time series) of each voxel into a scalar measure of activity or connectivity (LAAM-based FC, ReHO, and fALFF). (3) Feature selection, which involved computing for each voxel site its saliency as the Pearson's correlation coefficient (r) between two vectors, the first is composed the class labels of all the subjects, the second is composed of the voxel value of the scalar measure of activity or connectivity across all subjects. (4) We select the n voxel sites with greatest absolute r, instead of computing some threshold on the empirical distribution of the absolute r. We performed the classification experiments for the between-group comparisons of SZAH versus SZNAH and SZAH versus HC. For comparison, we also looked at classification performance for SZNAH versus HC and SZ versus HC. For each two-class classification problem, the feature selection process provides brain region localizations that may provide insights about AH pathophysiology. We provide more details for each of these steps below.

3.1. *Rationale for the approach*

Before we present the details of the computational procedures, we will give an overall justification of the approach applied, signaling the points of departure from traditional inference-based approaches. Traditionally, in brain imaging, statistical inference approaches are used to detect significant differences between data from different populations, such as in voxel-based morphometry (VBM) or analysis of fMRI task-based data. The process is similar to alarm raising, failure detection, or target detection, which represent outlier detection problems, i.e. involving identification of items that do not comply with the input data distribution and fall outside the expected pattern. In this traditional approach, the problem is stated at the voxel level. The decision about whether to reject the null hypothesis (of no difference between groups) is made at each voxel independently. When the null hypothesis model is well known, the problem at each voxel is thereby reduced to the computation of a single threshold. When the number of tests is large, correction for multiple comparisons avoids false positives due to randomness. However, multiple comparisons corrections may also limit detection of real signal by increasing the risk of false negatives, or type II error.

Machine learning, by contrast, offers a more holistic approach, whereby the aim is to make a decision about the subject as an entity, i.e. is the

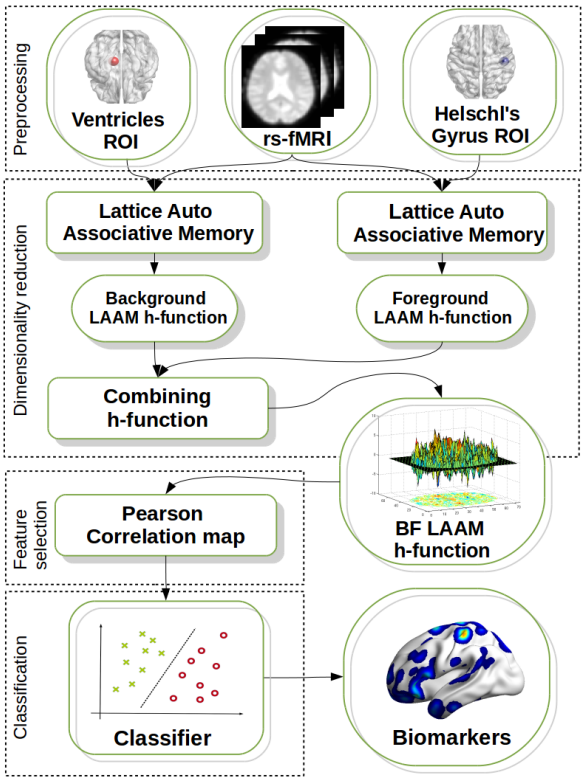

Fig. 1. Analysis pipeline for the background/foreground (BF)-LAAM-based FC approach. (1) rsfMRI data were preprocessed, and time series extracted from the specific background (cerebrospinal fluid, CSF) and foreground (right or left Heschl's gyrus) regions of interest (RoIs). (2) We then performed dimensionality reduction, reducing the high dimensionality time series data into LAAM-based FC measures. (3) We performed feature selection and extraction, using the Pearson's correlation coefficient (r) between the voxel value across subjects and the class label as a saliency measure to select the voxel sites with the greatest discriminative power. (4) We performed classification using support vector machines (SVM), and generate spatial maps showing the voxel sites with the features that are most highly discriminative.

person diseased or not? This approach places less importance on whether a statistically significant difference exists at any particular voxel. Rather than attributing to any voxel the credit for the decision, the goal of data processing is to extract informative features that contribute to the overall classification performance. In the current experiment, we are also interested in being able to identify localization information. Therefore, we look for features that map onto voxel sites that carry some anatomical meaning. This condition provides natural constraints to feature selection, and we select voxel sites on the basis of measures that are most salient in making a holistic decision about the subject. In such a process of feature selection, threshold-based decisions and multiple comparisons correction algorithms do not apply.

Finally, we must take into account that fMRI data, which consist of time series, are characterized by high dimensionality of information at each voxel. For computation of the significance measure it is necessary to reduce such data to a low-dimensional representation, e.g. a scalar value. To this end, we computed FC measures and LA measures at each voxel. For FC we applied a novel lattice computing approach. The impetus for an alternative connectivity measure arose from the relative lack of robust group-wise connectivity results found by conventional linear correlation in our previous work.[81] As we already touch upon in the introduction, LAAMs can serve as a nonlinear measure of connectivity. The construction of LAAMs is equivalent to the process of embedding data within a simplex (m-simplex is the convex hull of $m+1$ affine independent points, which are the vertices of the simplex; in this way, a 1-simplex is a line segment, a 2-simplex is a triangle and a 3-simplex is a tetrahedron, etc.)[78]; so

that transformations are naturally bounded and projected into the simplex boundaries. Because of their unique geometric architecture, LAAMs: (1) remove the effect of data outliers that can give rise to undesired connectivity,[10,28] (2) are robust to specific dilative and erosive types of noise to which fMRI data are vulnerable,[75,77,79] and (3) contain maximally discriminant information within the convex transformations of the data.[30] While we do not expect LAAM-based FC to reproduce exactly the findings of methods using Pearson's correlation coefficient, the LAAM-based findings may provide an alternative and complementary view of the data. In addition to LAAM-based FC, we also extract LA features, which measure the activity at a voxel or regional level. We expect that these local measures may reveal discriminant spatial distribution of the neural activity between populations.

3.2. *Preprocessing*

Data preprocessing began with skull removal using the brain extraction tool (BET) from FSL (http://www.fmrib.ox.ac.uk/fsl/). Images were manually oriented to the AC-PC line. The functional images were coregistered to the T1-weighted anatomical image. Using the Data Processing Assistant for Resting-State fMRI (DPARSF) (http://www.restfmri.net/forum/DPARSF) software package, the functional images were slice timing corrected, motion corrected (using a least squares approach and a 6-parameter spatial transformation), smoothed (FWHM = 4 mm), spatially normalized to the MNI template (resampling voxel size = 3 mm × 3 mm × 3 mm), temporally band pass filtered (0.01–0.08 Hz) to remove very low frequency physiological noise and high frequency noise from non-neurological sources, and removed of linear trends. Mean BOLD time courses for head motion, global brain signal, white matter, and CSF were regressed out before FC analysis. All the subjects had less than 3 mm maximum displacement and less than 3° of angular motion.

3.3. *Dimensionality reduction*

Each voxel contains fMRI time series data, which have high dimensionality. Prior to feature selection and extraction, the data need to be reduced to a low-dimensional representation, e.g. a scalar value. To this end, we computed FC measures and LA measures at each voxel.

3.3.1. *FC measures derived from LAAMs*

Conventionally, FC is calculated as the time course correlation between a target ROI and other brain voxels. By contrast, in a lattice computing approach to FC, fMRI time series are stored as LAAMs, and FC is defined as the recall error, which is the distance between the expected and actual recall pattern when presenting the input to the memory.

Given a set of input/output pairs of real valued patterns $(X, Y) = \{(\mathbf{x}^\xi, \mathbf{y}^\xi)\}_{\xi=1}^k$, Lattice Hetero-Associative Memories (LHAM) are the morphological counterpart of the linear associative memories, defined by exchanging the conventional multiplication and addition operators by minimum/maximum and addition operators, respectively, i.e. defining the dual lattice dilative and erosive matrix multiplications $\boxtimes$ and $\boxtimes$. Two dual constructions of LHAMs were originally proposed in Refs. 77 and 79: erosive LAM $W_{XY} = \bigwedge_{\xi=1}^k [\mathbf{y}^\xi \times (-\mathbf{x}^\xi)']$, and dilative LAM $M_{XY} = \bigvee_{\xi=1}^k [\mathbf{y}^\xi \times (-\mathbf{x}^\xi)']$. In these expressions, operator $\times$ can be any of the $\boxtimes$ or $\boxtimes$ operators, since $\mathbf{y}^\xi \boxtimes (-\mathbf{x}^\xi)' = \mathbf{y}^\xi \boxtimes (-\mathbf{x}^\xi)'$. A special case of LHAM happens when $X = Y$, then W_{XX} and M_{XX}; this is called LAAMs. LAAMs have been applied to hyperspectral endmember induction,[29] brain fMRI data segmentation,[30] and pattern classification based on the LAAM's recall error measured by the Chebyshev distance.[87] Given dilative LAAM M_{XX}, the recall of input of vector $\mathbf{x}$ is $\mathbf{x}_M^\# = M_{XX} \boxtimes \mathbf{x}$, and the recall error measured by the Chebyshev's distance:

$$h_X(\mathbf{x}) = d_C(\mathbf{x}^\#, \mathbf{x}), \tag{1}$$

where $d_C(\mathbf{a}, \mathbf{b}) = \bigvee_{i=1}^n |a_i - b_i|$, is the Chebyshev distance between two vectors. Function $h_X(\mathbf{x})$, which is the one-sided (OS)-LAAM h-function, can be used as a projection function from the high dimensional pattern space to a scalar magnitude. The erosive memory W_{XX} recall, i.e. $\mathbf{x}_W^\# = W_{XX} \boxtimes \mathbf{x}$, could be used alternatively.

A Background/Foreground (BF)-LAAM h-function is constructed by two OS-LAAM h-functions h_B and h_F, induced by dilative LAAMs M_{BB} and M_{FF} constructed on different training sets, i.e. background B and foreground F, respectively. We define

the BF-LAAM h-function $h_r(\mathbf{x})$ combining both h_B and h_F as follows:

$$h_r(\mathbf{x}) = h_F(\mathbf{x}) - h_B(\mathbf{x}), \tag{2}$$

which is positive for $\mathbf{x} \in \mathcal{F}(B)$, and negative for $\mathbf{x} \in \mathcal{F}(F)$, where $\mathcal{F}(X)$ is the set of fixed points of M_{XX}. Therefore, $h_r(\mathbf{x})$ is a discriminant function such that $h_r(\mathbf{x}) > 0$ corresponds to data samples in the background class, and $h_r(\mathbf{x}) < 0$ to data samples in the foreground class. The decision boundary is such that $h_r(\mathbf{x}) = 0$.

When dealing with fMRI data, the training datasets correspond to brain ROI time series. Computing either the OS or the BF-LAAM h-function for each voxel in an fMRI volume produces a scalar valued 3D h-map over the brain volume, which is a measure of the FC with this ROI used as the basis for feature selection and extraction for classification.

Here, we performed connectivity analysis to find the functional networks connected to the left (LHG) and right Heschl's gyrus (RHG) (Fig. 2) for each subject, following previous statistical inference works on correlation-based FC.[81] We computed the OS-LAAM h-function, for which the training dataset X are the fMRI time series in the selected ROI. We also computed the BF-LAAM h-function, where the background training dataset B corresponds to the CSF ROI extracted from the brain ventricle voxels

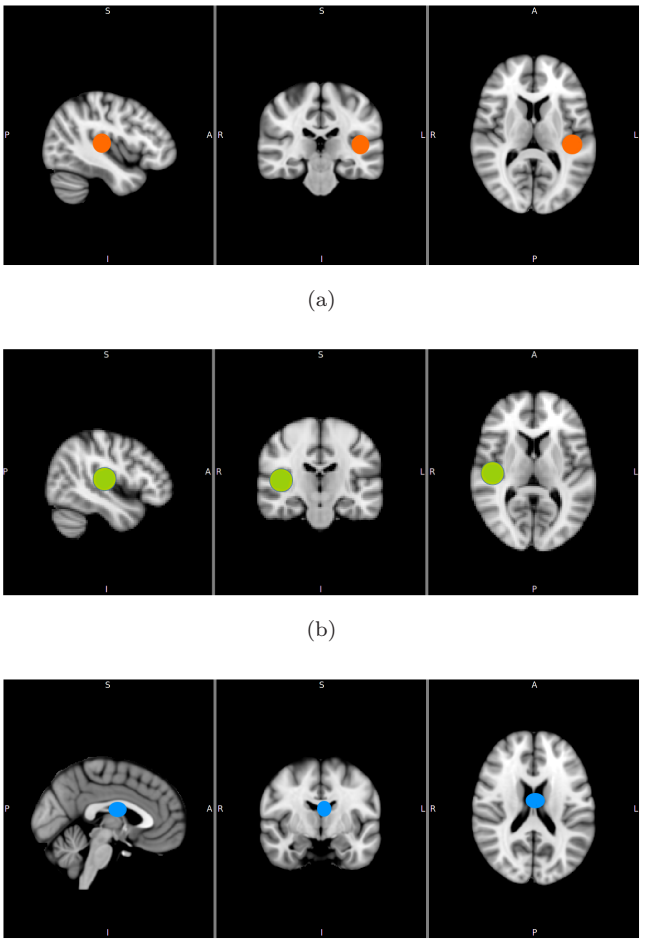

Fig. 2. The ROIs used for LAAM based connectivity analysis. The fMRI time series from LHG (10 mm, MNI coordinates $[-42, -26, 10]$) (a) and RHG (10 mm, MNI coordinates $[46, -20, 8]$) (b) were used to compute the left and right OS-LAAM h-functions, respectively. We also computed the BF-LAAM h-functions, where the fMRI time series from the CSF (10 mm, MNI coordinates $[-15, -26, 10]$) (c) was set as the background training dataset and the fMRI time series from the LHG (a) or RHG (b) were set as the foreground training dataset.

(MNI coordinates $-15, -26, 10$), and the Foreground training dataset F is the average time signal from a selection of voxels in the LHG or the RHG (MNI coordinates $46, -20, 8$).[81]

3.3.2. *Local fMRI activity measures*

We also computed local fMRI activity measures, which correspond to values measuring local properties of the signal:

(1) ReHo is a local measure of the homogeneity of brain activity which computes the Kendall's Coefficient of Concordance (W) between the time series of a given voxel and its nearest neighbors.[104] Given a collection of vectors $\{\mathbf{x}_j \in \mathbb{R}^n\}_{j=1}^k$, which in our study correspond to voxel time series, the Kendall's Coefficient of Concordance[46] is computed as follows:

$$W = \frac{\sum_i (R_i)^2 - n(\overline{R})^2}{\frac{1}{12}k^2(n^3 - n)}, \tag{3}$$

where $R_i = \sum_{j=1}^k r_{ij}$, and r_{ij} is the rank of the ith time point in the jth voxel. The value of W ranges from 0 to 1. $\overline{R} = (n+1)k/2$ is the mean of the R_i. In our study W is used as a measure of the homogeneity of the neighborhood of a voxel in the ReHo measure. We apply a conventional 3D neighborhood, which is a 3D window around the voxel of dimensions $3 \times 3 \times 3\,\text{mm}^3$. The W values are standardized and smoothed (4 mm FWHM) to build a voxel-based scalar map for each subject.

(2) ALFF[103] and fALFF[107] are measures of the strength of low LFOs of the BOLD signal. ALFF is defined as the total power within the frequency range between 0.01 and 0.1 Hz. fALFF is the relative contribution of specific LFO to the power of whole frequency range, defined as the power within the low-frequency range (0.01–0.1 Hz) split by the total power in the entire detectable frequency range.[108] In the current paper, we focus on fALFF.

3.4. *Feature selection and extraction*

Feature extraction gathers the values of the most salient voxels into a feature vector, used for classification. For this step, we computed the voxel saliency map. That is, for each voxel site, we computed the Pearson's Correlation Coefficient (r) between its vector of values of the scalar feature across subjects with the class label categorical variable.

The Pearson's Correlation Coefficient (r) is a measure of the linear correlation between two random variables samples given by vectors $\mathbf{x}, \mathbf{y} \in \mathbb{R}^n$, it is computed as follows:

$$r = \frac{n\left(\sum_i x_i y_i\right) - \left(\sum_i x_i\right)\left(\sum_i y_i\right)}{\sqrt{\left[n\sum_i x_i^2 - \left(\sum_i x_i\right)^2\right]\left[n\sum_i y_i^2 - \left(\sum_i y_i\right)^2\right]}}, \tag{4}$$

so that $r \in [-1, 1]$, $r = 1$ means that two variables have total positive correlation, and $r = -1$ means that they have total negative correlation, and $r = 0$ that there is no correlation at all. We use r between the voxel value across subjects and the class label variable as a saliency measure to select the voxel sites with the greatest discriminative power. Voxel sites with near zero r are not informative and can be discarded. Both positive or negative r values mean that the voxel site value can be an informative feature for classification.

Each classification experiment involves a separate saliency map, that is one per each scalar feature map and classification problem: We have explored the discrimination between each possible pair of classes: SZAH versus SZNAH, SZAH versus HC, SZNAH versus HC, and HC versus schizophrenia.

Feature selection looks for the n voxel sites with the largest absolute r values. Experiments are performed considering the following feature vector sizes: $n = 500, 1000, 5000, 10{,}000$. Figures 3 and 4 show the regional localizations corresponding to feature vector dimension 1000 for the voxel saliency 3-dimensional maps obtained from OS LAAM h-function, BF LAAM h-function, and correlation-based FC computed using either LHG or RHG ROIs, respectively. The brain regions were identified using the Harvard Oxford cortical atlas via the atlas query tool in FSL (http://www.fmrib.ox.ac.uk/fsl/). We show the localization results for the 1000 feature vector dimension because classification results across feature vector dimensions are similar, and the clusters in the 1000 dimension experiments are larger and thus easier to visualize.

Feature extraction builds the actual feature vectors extracting the selected voxel site values from

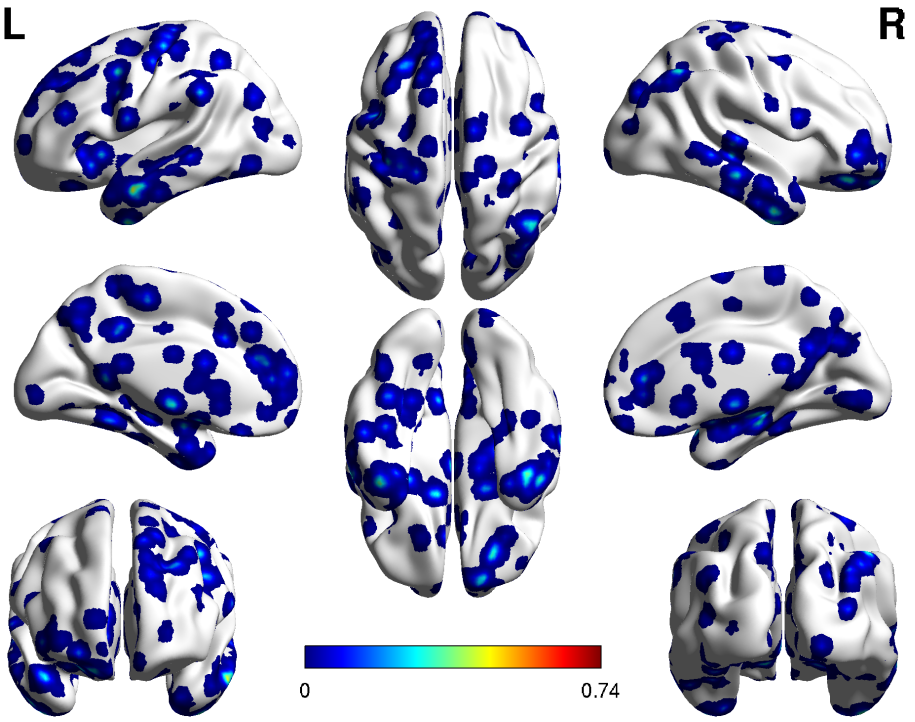

Fig. 3. (Color online) Localization of feature voxel sites selected from the BF-LAAM h-function map with foreground seed extracted from the LHG ROI, when discriminating SZAH from SZnAH populations. Colorbar is proportional to voxel saliency.

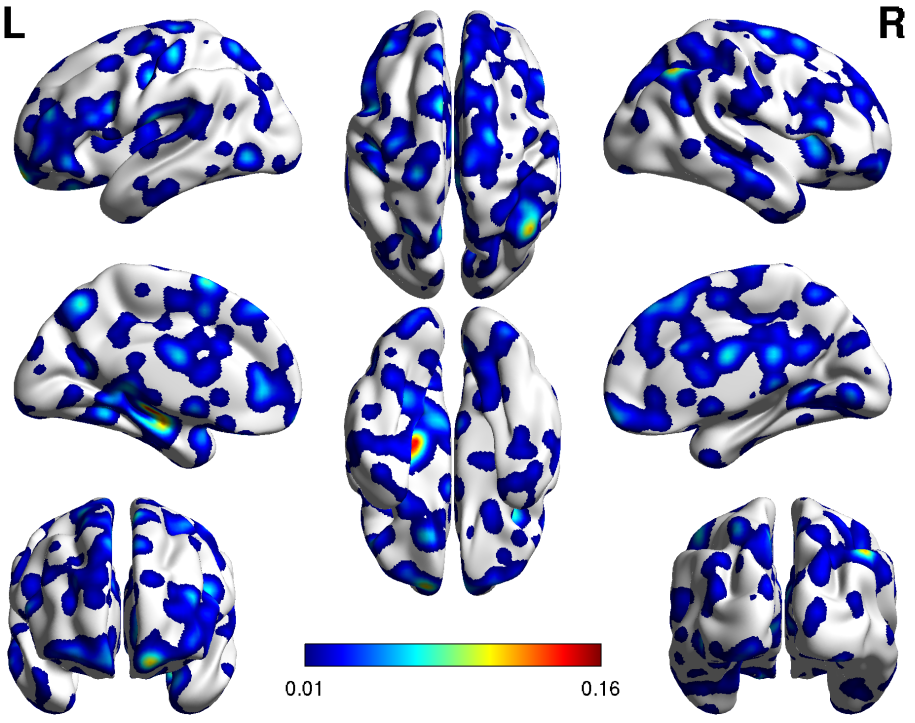

Fig. 4. (Color online) Localization of feature voxel sites selected from the BF-LAAM h-function map with foreground seed extracted from the RHG ROI, when discriminating SZAH from SZnAH populations. Colorbar is proportional to voxel saliency.

the scalar feature map of each subject. Therefore, we have separate feature datasets for each classification experiment, scalar feature (i.e. FC and local activity measures), and feature vector size.

3.5. *Classification by SVM*

SVM,[8,53,90] have become the de facto standard classifier construction method..[9,26,43,88,99] Given a training dataset composed of n-dimensional feature vectors $\mathbf{x}_i \in \mathbb{R}^n$, $i = 1, \ldots, l$ and corresponding class labels $y_i \in \{-1, 1\}$, (patients are labeled as -1 and control subject as 1), the objective is to build using training data a discriminating function $f(\mathbf{x}) = \text{sign}(\sum \alpha_i y_i K(\mathbf{s}_i, \mathbf{x}) + w_0)$, that will correctly classify new examples $(\mathbf{x}, y)$. In this expression, $K(.,.)$ is a kernel function, α_i is a weight derived from the SVM process, and the $\mathbf{s}_i$ are the so-called support vectors. SVM training seeks the set of support vectors providing the decision hyperplane that is maximally distant from the samples of the two classes. When no linear separation of the training data is possible, the kernel transformation $K(\mathbf{x}_i, \mathbf{x}_j) \equiv \phi(\mathbf{x}_i)^T \phi(\mathbf{x}_j)$ enables mapping of the decision hyperplane into a nonlinear decision boundary in the higher dimensional space defined by the implicit function $\phi(\mathbf{x}_i)$. This higher dimensional space may be even of infinite dimension for some kernel functions, such as the Radial Basis Function (RBF) kernel. Training is achieved by solving the following optimization problem $\min_{w,b,\xi} \frac{1}{2}\mathbf{w}^T\mathbf{w} + C\sum_{i=1}^{l} \boldsymbol{\xi}_i$, subject to $y_i(\mathbf{w}^T\phi(\mathbf{x}_i) + b) \geq (1 - \xi_i)$, $\xi_i \geq 0, i = 1, 2, \ldots, n$. In fact, $C > 0$ is a regularization parameter used to balance the model complexity and the training error. The dual optimization problem is formulated as $\min_\alpha \frac{1}{2}\boldsymbol{\alpha}^T\mathbf{Q}\boldsymbol{\alpha} - \mathbf{e}^T\boldsymbol{\alpha}$, subject to $\mathbf{y}^T\boldsymbol{\alpha} = 0$, $0 \leq \alpha_i \leq C$, $i = 1, \ldots, l$, where $\mathbf{e}$ is the vector of all ones, and $\mathbf{Q}$ is an $l \times l$ positive semi-definite matrix, such that $Q_{ij} \equiv y_i y_j K(\mathbf{x}_i, \mathbf{x}_j)$. In this study we use the linear kernel, which is the minimal complexity approach requiring no model selection procedures for parameter tuning. Performing model selection of kernel parameters may introduce an additional bias in the results, independent from the significance of the extracted features. Solving the dual problem, we obtain the contribution of specific sample vectors, the support vectors, to the construction of the decision function. In some cases it is possible to obtain qualitative information from the support vectors, when they can be interpreted as representatives of desired features.

We applied a 10-fold cross-validation strategy, repeated 100 times. Thus, before applying SVM for classification, we split the data into 10 sets. We used the first nine sets to train the classifier, and the 10th set to test the data using the constructed classifier. The procedure is repeated using each partition as test set and the remaining as training set.

4. Results

Tables 1–3 contain the average accuracy, sensitivity, and specificity, respectively, classification of cross-validation experiments. The columns in each table correspond to specific sizes of the feature vectors. Rows are grouped by classification problem, i.e. HC versus SZAH, HC versus SZ, HC versus SZnAH, and SZnAH versus SZAH. The HG column specifies which hemisphere Heschl's Gyrus has been used as seed ROI for FC feature extraction, either left (L) or right (R). Rows correspond to the specific scalar feature method and specific conditions. 'OS-LAMM' and 'BF-LAAM' rows give the results of corresponding h-maps applied to compute the FC measures to either the LHG or RHG. 'ReHo', 'ALFF' and 'fALFF' mean that the scalar maps are computed as the corresponding local functional activity measures. Two-sided t-tests were computed on all the stored results of the 10-fold cross-validation.

4.1. *Classification performance according to group contrasts*

SZAH versus SZNAH:

- FC:
  - BF-LAAM: Features from RHG-seeded FC were more discriminant than features from LHG-seeded FC ($p < 0.01$). Both achieved 100% accuracy at feature vector dimension 500, but LHG-seeded FC degraded strongly with increasing vector dimension, due to decreasing specificity.
  - OS-LAAM: there were no significant differences in performance between RHG-seeded and LHG-seeded FC ($p > 0.01$). Both of these features achieved 100% sensitivity but poorer specificity.

Table 1. Average accuracy of cross-validation results, feature vector size *per* columns.

	Measure	Feat. Map.	HG	500	1000	5000	10,000
SZAH versus SZNAH	FC	OS-LAAM	L	**97.5**	**97.5**	**97.5**	**92.5**
			R	**92.5**	**92.5**	**95**	**95.2**
		BF-LAAM	L	**100**	**97.5**	**95**	**90**
			R	**100**	**100**	**100**	**100**
	LA	ReHo	—	**100**	**100**	**100**	**100**
		ALFF	—	85	87.5	**92.5**	**92.5**
		fALFF	—	**97.5**	**100**	**100**	**97.5**
SZAH versus HC	FC	OS-LAAM	L	43.7	42.7	30.7	28.3
			R	52.3	50	33	28
		BF-LAAM	L	**96.7**	**98**	**96.3**	**93**
			R	**98.3**	**96**	**92.7**	**93**
	LA	ReHo	—	**98**	**98.3**	**96.7**	**96.6**
		ALFF	—	48.7	49	30.3	31.7
		fALFF	—	**100**	**100**	**98.3**	**98.3**
SZNAH versus HC	FC	OS-LAAM	L	65	63	59.5	55
			R	74	70	60	55
		BF-LAAM	L	**100**	**100**	**95.5**	**93**
			R	**100**	**98**	**95.5**	**93.5**
	LA	ReHo	—	**97.5**	**98**	**95.5**	**96**
		ALFF	—	78	76	62	53
		fALFF	—	**100**	**100**	**100**	**100**
SZ versus HC	FC	OS-LAAM	L	32.4	31	26	25
			R	41.4	36.7	26.9	25.2
		BF-LAAM	L	**95.5**	**97.1**	88.6	85.7
			R	**94.3**	**91.2**	86.7	87.1
	LA	ReHo	—	**95.7**	**95.7**	**97**	**95.5**
		ALFF	—	48.8	42.9	35.2	35.2
		fALFF	—	**98.5**	**100**	**97.1**	**97.1**

Note: Rows correspond to scalar feature mappings. Column HG indicates the left (L) or right (R) Heschl's Gyrus ROI. Results above 90% are highlighted in bold. Key to abbreviations: FC = Functional connectivity, LA = Local Activity, OS-LAAM = one-sided lattice auto-associative memories, BF-LAAM = background/foreground lattice auto-associative memories, ReHo = regional homogeneity, ALFF = amplitude of low frequency fluctuations, fALFF = fractional amplitude of low frequency fluctuations.

- LA: ReHo achieved 100% accuracy, sensitivity, and specificity across all four tested feature vector dimensions. A two-sided t-test revealed no statistically significant differences between fALFF and ReHo ($p > 0.01$). On the other hand, ALFF performed significantly worse than ReHo ($p < 0.01$). This appears to be due to low specificity (75–85%) in spite of high sensitivity (96.7–100%).

SZAH versus HC:

- FC:
  - BF-LAAM: There were no significant differences between RHG-seeded FC and LHG-seeded FC ($p > 0.01$).
  - OS-LAAM: There was no difference between RHG- and LHG-seeded FC ($p > 0.01$); both performed poorly in the ranges of 28–52.3% and 28.3–43.7% accuracy, respectively, due to very low sensitivity.
- LA: fALFF and ReHo reached 100% and 98.3% accuracy, respectively. Despite having close values, statistically, fALFF showed higher discriminative

Table 2. Average sensitivity of cross-validation results, feature vector size *per* columns.

	Measure	Feat. Map.	HG	500	1000	5000	10,000
SZAH versus SZNAH	FC	OS-LAAM	L	**100**	**100**	**100**	**100**
			R	**100**	**100**	**100**	**100**
		BF-LAAM	L	**100**	**100**	**100**	**100**
			R	**100**	**100**	**100**	**100**
	LA	ReHo	—	**100**	**100**	**100**	**100**
		ALFF	—	**96.7**	**96.7**	**100**	**100**
		fALFF	—	**100**	**100**	**100**	**100**
SZAH versus HC	FC	OS-LAAM	L	28.3	21.7	11.7	8.3
			R	38.3	30	18.3	10
		BF-LAAM	L	**96.7**	**96.7**	**93.3**	85
			R	**96.7**	**93.3**	**91.7**	**93.3**
	LA	ReHo	—	**100**	**100**	**96.6**	**96.7**
		ALFF	—	45	41.7	21.7	18.3
		fALFF	—	**100**	**100**	**100**	**100**
SZNAH versus HC	FC	OS-LAAM	L	40	40	20	15
			R	50	40	25	20
		BF-LAAM	L	**100**	**100**	**90**	80
			R	**100**	**95**	**90**	85
	LA	ReHo	—	**100**	**100**	**95**	**95**
		ALFF	—	60	50	30	20
		fALFF	—	**100**	**100**	**100**	**100**
SZ versus HC	FC	OS-LAAM	L	30	27.5	17.5	20
			R	40	35	25	22.5
		BF-LAAM	L	**97.5**	**100**	**95**	**92.5**
			R	**95**	**95**	**90**	**92.5**
	LA	ReHo	—	**100**	**100**	**96.6**	**96.7**
		ALFF	—	47.5	45	37.5	35
		fALFF	—	**97.5**	**100**	**97.5**	**97.5**

Note: Rows correspond to scalar feature mappings. Column HG indicates the left (L) or right (R) Heschl's Gyrus ROI. Results above 90% are highlighted in bold. Key to abbreviations: FC = Functional connectivity, LA = Local Activity, OS-LAAM = one-sided lattice auto-associative memories, BF-LAAM = background/foreground lattice auto-associative memories, ReHo = regional homogeneity, ALFF = amplitude of low frequency fluctuations, fALFF = fractional amplitude of low frequency fluctuations.

ability than ReHo and BF-LAAM ($p < 0.01$). On the other hand, ALFF performed poorly due to low sensitivity.

SZNAH versus HC:

- FC:
  - — BF-LAAM: There were no significant differences between RHG-seeded FC and LHG-seeded FC ($p > 0.01$), both achieved 100% accuracy, sensitivity, and specificity.
  - — OS-LAAM: There were no significant differences between RHG-seeded FC and LHG-seeded FC ($p > 0.01$), both showed poor discriminative ability, with accuracy below 80%, at best. Specifically had very low sensitivity.
- LA: ReHo showed 95.5–98% accuracy, 95-100% sensitivity, and 96.7% specificity. ALFF showed

Table 3. Average specificity of cross-validation results, feature vector size *per* columns.

	Measure	Feat. Map.	HG	500	1000	5000	10,000
SZAH versus SZNAH	FC	OS-LAAM	L	**95**	**95**	**95**	85
			R	80	85	**90**	85
		BF-LAAM	L	**100**	**95**	**90**	75
			R	**100**	**100**	**100**	**100**
	LA	ReHo	—	**100**	**100**	**100**	**100**
		ALFF	—	75	75	85	85
		fALFF	—	**95**	**100**	**100**	**95**
SZAH versus HC	FC	OS-LAAM	L	63.3	71.7	51.7	51.7
			R	70	75	53.3	50
		BF-LAAM	L	**100**	**100**	**100**	**100**
			R	**100**	**100**	**97.7**	**96.7**
	LA	ReHo	—	**96.7**	**96.6**	**96.7**	**96.7**
		ALFF	—	65	58.3	46.7	51.7
		fALFF	—	**100**	**100**	**96.7**	**96.7**
SZNAH versus HC	FC	OS-LAAM	L	81.7	83.3	81.7	78.3
			R	**90**	**90**	81.7	76.7
		BF-LAAM	L	**100**	**100**	**100**	**100**
			R	**100**	**100**	**100**	**100**
	LA	ReHo	—	**96.7**	**96.7**	**96.7**	**96.7**
		ALFF	—	**90**	**93.3**	83.3	73.3
		fALFF	—	**100**	**100**	**100**	**100**
SZ versus HC	FC	OS-LAAM	L	55	40	38.3	40
			R	46.7	45	36.7	35
		BF-LAAM	L	**93.3**	**95**	83.3	76.7
			R	**96.7**	**90**	85	83.3
	LA	ReHo	—	**96.7**	**96.7**	**96.7**	**96.7**
		ALFF	—	56.7	48.3	40	41.7
		fALFF	—	**100**	**100**	**96.7**	**96.7**

Note: Rows correspond to scalar feature mappings. Column HG indicates the left (L) or right (R) Heschl's Gyrus ROI. Results above 90% are highlighted in bold. Key to abbreviations: FC = Functional connectivity, LA = Local Activity, OS-LAAM = one-sided lattice auto-associative memories, BF-LAAM = background/foreground lattice auto-associative memories, ReHo = regional homogeneity, ALFF = amplitude of low frequency fluctuations, fALFF = fractional amplitude of low frequency fluctuations.

poor discriminative ability, with 78% accuracy at best, due to low sensitivity. fALFF achieved 100% accuracy, sensitivity, and specificity across all four feature vector dimensions, significantly better than ReHo ($p < 0.01$).

SZ versus HC:

- FC:
  - — BF-LAAM: Though LHG-seeded FC provide some improvement over RHG-seeded FC, the difference was not statistically significant ($p > 0.01$). Both approaches give high sensitivities and low specificities.
  - — OS-LAAM: Both RHG-seeded FC and LHG-seeded FC showed poor performance, with both low accuracy and sensitivity.
- LA: ALFF showed poor discriminative ability. fALFF achieved 100% accuracy, sensitivity, and specificity and performed significantly better than ReHo ($p < 0.01$), which achieved 97% accuracy.

Table 4. Cortical brain regions of the feature voxel sites corresponding to BF-LAAM h-map feature vector of size 1000, for the classification of SZAH versus SZNAH.

BF-LAAM LHG		Coordinates				BF-LAAM RHG		Coordinates			
Region	H	CS	x	y	z	Region	H	CS	x	y	z
Middle Frontal Gyrus	L	10	−36	33	45	Frontal pole	L/R	7/11	−15/6	60/69	−18/−9
IFG	L	10	−60	18	−3	Superior frontal gyrus	L	5	−3	36	48
MTG	L	33	−57	−6	−27	Superior temporal gyrus	L	5	−72	−24	6
Temporal pole	R	11	30	27	−36	Postcentral gyrus	L	7	−45	−33	63
Precentral gyrus	L	10	−21	−24	63	Juxtapositional lobule cortex		8	0	9	66
Parahippocampal gyrus	R	15	27	−24	−15	Angular gyrus	R	5	51	−54	48
						Cingulate gyrus	R	5	6	−33	18
						Lateral occipital cortex	R	6	42	−63	45
						Occipital fusiform gyrus	L	5	−36	−75	−9
						Parahippocampal gyrus	L	21	−21	−12	−21

Note: Regions highlighted in bold typeface have also been reported in Ref. 81. CS = Cluster size, H = Brain hemisphere, L = Left, R = Right.

Table 5. Cortical brain regions of the feature voxel sites corresponding to ReHo and fALFF feature vectors of size 1000, for the classification of SZAH versus SZNAH.

ReHo		Coordinates				fALFF		Coordinates			
Region	H	CS	x	y	z	Region	H	CS	x	y	z
IFG	L	25	−54	27	24	Frontal medial cortex	R	28	12	39	−15
Frontal orbital cortex	L	37	−48	24	−9	Frontal pole	R	43	21	54	−15
Frontal operculum cortex	R	14	42	24	6	MTG	L/R	17/7	−57/57	−39/−42	−12/−12
Superior frontal gyrus	L	13	−18	6	66	Central opercular cortex	L	14	−36	9	12
Superior temporal gyrus	L	18	−69	−6	0	Insular cortex	R	14	27	18	0
Inferior temporal gyrus	R	13	42	0	−51	Cingulate gyrus	L	7	−15	9	30
Temporal pole	L/R	14/16	−45/39	9/6	−36/−39	Paracingulate gyrus	L	14	−15	30	24
Precentral gyrus	L/R	21	18	−18	72						
Parietal operculum cortex	R	13	51	−30	27						
Supramarginal gyrus	R	13	30	−48	33						
Cingulate gyrus, posterior division	R	20	9	−39	3						
Subcallosal cortex	L	36	−3	30	0						
Precentral gyrus	L	41	−30	−21	48						

Note: CS = Cluster size, H = Brain hemisphere, L = Left, R = Right.

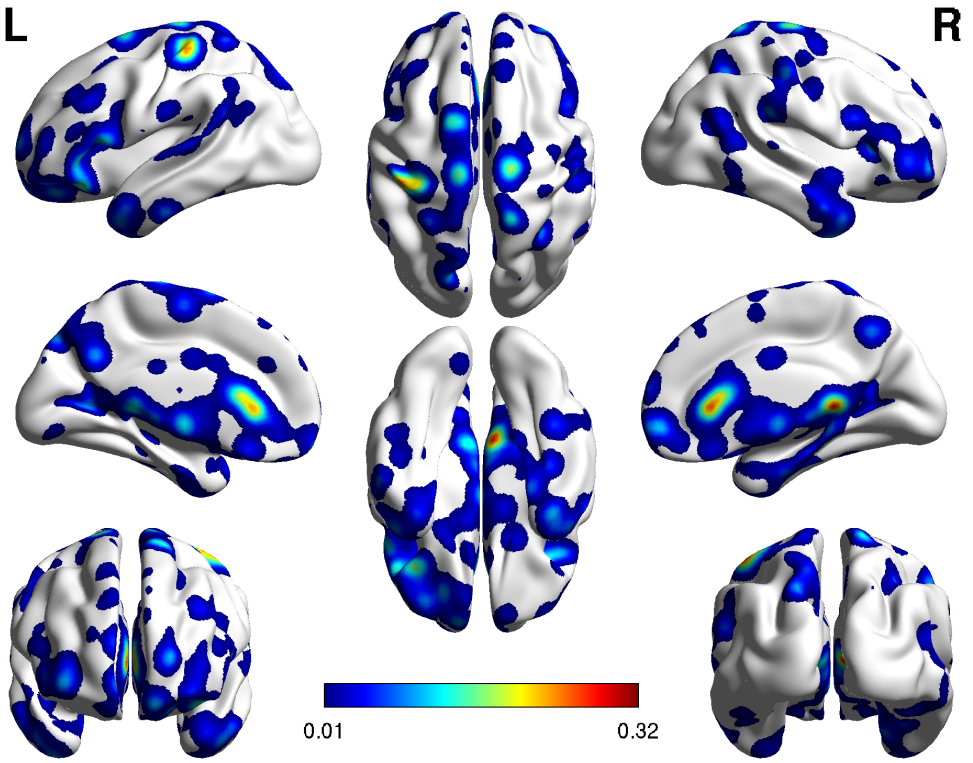

Fig. 5. (Color online) Localization of feature voxel sites selected from the ReHo, when discriminating SZAH from SZnAH populations. Colorbar is proportional to voxel saliency.

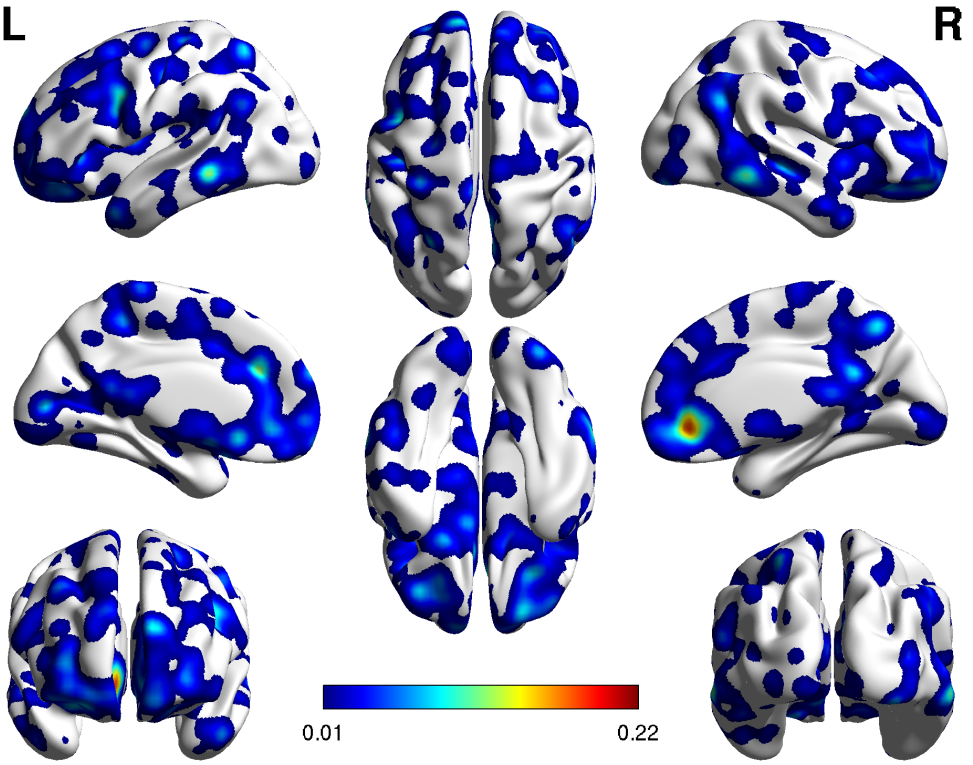

Fig. 6. (Color online) Localization of feature voxel sites selected from the fALFF, when discriminating SZAH from SZnAH populations. Colorbar is proportional to voxel saliency.

4.2. *Results according to feature vector dimension*

An F-test performed on the accuracy of all methods aggregated by feature vector size shows that there is significant differences due to dimensionality ($p < 0.01$). *Post-hoc* t-tests show that the dimension size of 500 provided the best classification performance ($p < 0.001$). The feature vectors of dimension 10,000 tended to show the worst classification results.

When discriminating between the SZAH and SZNAH groups, dimensionality did not seem to make a difference with LAAM-based FC measures or with ReHo and fALFF; there was 100% accuracy across all four feature vector dimension sizes tested. The exception was with ALFF, where lower dimensionality (500, 1000) yielded accuracy of 96.7% instead of 100%.

4.3. *Cortical brain regions associated with discriminant voxels*

Tables 4 and 5 list the cortical brain regions to which the discriminant features extracted from the BF-LAMM h-map and the ReHo and fALFF activity maps localized. Figures 3–6 show the cortical brain regions that were most discriminating between SZAH and SZNAH with the feature measures: LHG seeded BF-LAAM h-map 3, RHG-seeded BF-LAAM 4, ReHo 5, and fALFF 6, respectively, with feature vector size of 1000. Each figure presents eight views of the brain cortex, and the feature sites are projected over the cortex as colored regions following a color coding given by the colorbar, with colors corresponding to values of the voxel saliency. The range of values of the color bar change from one figure to another as the range of values of the voxels saliencies change from one classification problem to another.

5. Discussion and Conclusions

In this study, we investigated the discriminative value of LAAM-based FC measures as well as local fMRI activity measures (ReHo, ALFF, and fALFF) in differentiating schizophrenia patients with lifetime history of AH from schizophrenia patients without lifetime AH and HC. We found BF-LAAM, ReHo, and fALFF to provide the strongest classification performance in discriminating both SZAH from SZNAH and HC. The features extracted from the OS-LAAM h-maps and ALFF reached accuracy above 90% only in the SZAH versus SZNAH contrast.

Discriminating hallucinators

The classification performance for SZAH versus SZNAH was superior to that for SZAH versus HC. This was a surprising finding, as one might expect larger brain differences between patients and healthy individuals than between two groups of patients with the same diagnosis, and thus expect discrimination between SZAH and HC to be more robust. This was not the case. In fact, classification experiments on the discrimination of SZ versus HC showed the worst performance. From a purely computational perspective, the unequal sample sizes between the HC ($n = 28$) and schizophrenia ($n = 40$) groups may explain some, but not all, of the decrease in classification performance, because SVM is known to be sensitive to this feature of the data. The degradation in classification performance may also be due to the heterogeneity of the schizophrenia group, which consists of two subgroups (SZAH and SZNAH) which are already discriminable. Overall, however, these results suggests that FC and local fMRI activity differences associated with the presence or absence of lifetime AH history in patients with schizophrenia are valid biological measures upon which patients can be differentiated. That classification on the basis of AH outperformed classification according to the presence or absence of schizophrenic illness provides support for the National Institute of Mental Health (NIMH) Research Domain Criteria (RDoC) initiative[37,38] to find new, neuroscience-based frameworks for classifying mental illness, rather than confine study designs to traditional diagnostic categories.

Comparing FC features

Another surprising finding was the superiority of RHG relative to LHG seeded FC measures in discriminating SZAH from SZNAH. While the original study by members of our group[81] showed SZAH patients to have only LHG seeded FC abnormalities, and no RHG seeded FC abnormalities, the current analyses applying machine learning algorithms found RHG connectivity to show the best classification performance. Most accounts of AH pathogenesis focus on the role of the left hemisphere, where most speech and language functions are lateralized. Prosody and

emotional valence, by contrast, are lateralized in the right hemisphere. It has been argued that prosody is what causes one to perceive a thought as being one's own, and that changes in prosodic tone may cause inner speech to be misattributed and experienced as AH.[12] Our finding of stronger discriminative power of RHG seeded FC measures is in line with evidence for right auditory cortex dysfunction[58] and temporal lobe lateralization abnormalities[66,67] in schizophrenia patients with AH. The differences in the laterality of findings between the original and current studies may be due to signfiicant methodological differences in data analysis. For example, the current machine learning approach used BF-LAAM, a novel lattice-based measure, to compute FC. And as we describe in Sec. 1, LAAMs are highly robust to certain types of noise in rsfMRI. Importantly, in the current study, we applied a machine learning model, which makes more holistic decisions about the subject as an entity; this is a fundamentally different approach than traditional statistical inference methods, which rely on significance testing at the voxel level.

Feature localization and interpretation

We attribute high pathophysiological significance to the discriminant voxel sites achieving high classification results, and the brain localizations derived from the features with strong classification performance may have biological significance relative to the pathophysiology of AH. Specifically, BF-LAAM h-maps from both LHG and RHG seeds provide FC information which can be interpreted in the context of existing models of AH. Voxels localizing to the left IFG (or Broca's area) emerged as highly discriminant in classification experiments using LHG seeded FC. The left IFG was found to be significant in meta-analyses of AH activity[40,49] and is centrally featured in inner speech models of AH.[42] The IFG also plays a role in corollary discharge accounts of AH, along with auditory and speech regions in temporal cortex.[23] Voxels in temporal cortical regions were highly discriminant, with left middle temporal gyrus (MTG) and right temporal pole emerging as significant in LHG FC and left STG emerging in the LHG FC experiment. The finding of discriminant voxels in the parahippocampal gyrus is consistent with memory-based models of AH[94] and with the finding that AH in schizophrenia patients are consistently preceded by deactivation of the parahippocampal gyrus.[15,35] Of interest, our findings show Heschl's gyrus-parahippocampal gyrus FC abnormalities that are interhemispheric, i.e. RHG showed abnormal connectivity with left parahippocampal gyrus, and LHG showed abnormal connectivity with right parahippocampal gyrus. Finally, highly discriminate voxels were found in the cingulate cortex and frontal cortical regions; both of these regions feature prominently in AH models relating to a failure of top-down inhibitory control[3,36] as well as those involving source-monitoring deficits.[93] As can be seen, the FC information provided by BF-LAAM features is in agreement with the expected effects. Further detailed analysis may provide more light into the directions of these effects.

Comparing the group-wise LHG FC findings reported for SZAH versus SZNAH in Ref. 81 with the FC results from the current study (Table 4), we find only two regions — the left middle frontal gyrus and right parahippocampal gyrus — in common. As previously mentioned, significant differences in analytic approach may account for the lack of greater overlap in findings. In particular, the group-wise SZAH versus SZNAH findings in the original paper were less robust than those resulting from the AH covariate analysis in the same study. This may have been attributable to the relatively small sample size of the nonhallucinating group of patients, who are rarer in schizophrenia and thus more challenging to recruit. The current approach, which uses a FC measure based on nonlinear lattice computing, may be statistically more robust and less vulnerable to type II error. Notably, both the current study and analysis examining AH as a continuous variable in Ref. 81 show abnormal LHG seeded FC in left IFG (Broca's area), a speech/language region that is clearly important in several models of AH.

The ReHo map identifies regions of homogeneous activity, which may reflect the extent of synchronized neural activity within specific regions. ReHo showed strong classification performance in discriminating patients with and without AH history. Looking at the ReHo feature localizations in Table 5 we find many regions of the frontal, temporal, somatosensory, and the limbic system (cingulate gyrus and subcallosal cortex), covering the expected areas described by AH generation models. The fALFF map identifies voxels of high/low activity in the low frequency spectrum

of the signal. The regions reported in Table 5 also meet the expectation of the aforementioned models, including the language areas, the auditory perceptual areas as well as the emotional areas, and the insular cortex in charge of self-recognition.

Limitations

The current analysis did not take into account clinical or demographic variables other than schizophrenia diagnosis and lifetime history of AH. However, as described in the original paper,[81] the SZAH and SZNAH groups were clinically comparable. Improved preprocessing of rsfMRI data, for example, by applying innovative signal filtering algorithms for the removal of physiological noise,[73,74] may increase confidence in the biological significance of the reported findings. The application of machine learning to multiple imaging modalities rather than to rsfMRI data alone[69] would also help to confirm our results. In addition, classification could be further enhanced by innovative unsupervised[56,60] or supervised[4,39] approaches. Finally, while the brain localizations derived from features with strong classification performance provide information about brain areas that likely have biological relevance in AH pathophysiology, the discriminant voxels do not contain information about the directionality of connectivity (i.e. hyper- or hypoconnectivity) with LHG and RHG. In spite of these potential limitations, we demonstrate that classification using BF-LAAM-based functional connectivity, and local fMRI measures like ReHo and fALFF are extremely robust in discriminating SZAH from SZNAH and HC.

Conclusion

This study is the first to classify schizophrenia patients on the basis of lifetime AH by applying a machine learning approach to resting state fMRI data. Using a novel LAMM algorithm, in addition to measures of more local fMRI activity including ReH and FALFF, we demonstrate robust ability to discriminate schizophrenia patients with a history of AH from those who have never experienced AH. For all classification measures, classification according to the presence or absence of AH was superior to classification on the basis of psychiatric diagnosis, offering support for dimensional, symptom-based approaches. LAAM-based FC seeded in right hemisphere Heschl's gyrus showed stronger discriminative value than FC measures seeded in LHG, providing possible evidence in support of AH models that focus on right hemisphere brain abnormalities.

Acknowledgments

Darya Chyzhyk has been supported by a FPU grant from the Spanish MEC. Support from MICINN through project TIN2011-23823. GIC has grant IT874-13 from the Basque Governemnt, and participates at UIF 11/07 of UPV/EHU. Some of the funding programs are funded by FEDER.

References

1. H. Abdi, D. Valentin and B. Edelman, *Neural Networks*, *Sage University Paper Series on Quantitative Applications in the Social Sciences, series No.* 124 (Sage Publications, Inc., 1999).
2. H. Adeli and S. Hung, *Machine Learning — Neural Networks*, *Genetic Algorithms*, *and Fuzzy Systems* (John Wiley and Sons, New York, 1995).
3. P. Allen, F. Larøi, P. K. McGuire and A. Aleman, The hallucinating brain: A review of structural and functional neuroimaging studies of hallucinations, *Neurosci. & Biobehav. Rev.* **32**(1) (2008) 175–191.
4. B. Baruque, E. Corchado and H. Yin, The s2-ensemble fusion algorithm, *Int. J. Neural Syst.* **21**(6) (2011) 505–525.
5. R. Bentall and P. Slade, Reality testing and auditory hallucinations: A signal detection analysis, *B. J. Clin. Psychol.* **24**(3) (1985) 159–169.
6. G. Birkhoff, *Lattice Theory* (AMS Bookstore, 1995).
7. B. Biswal, F. Zerrin Yetkin, V. M. Haughton and J. S. Hyde, Functional connectivity in the motor cortex of resting human brain using echo-planar mri, *Magn. Reson. Med.* **34**(4) (1995) 537–541.
8. C. Burges, A tutorial on support vector machines for pattern recognition, *Data Mining Knowl. Discov.* **2**(2) (1998) 167–121.
9. F. Chu and L. Wang, Applications of support vector machines to cancer classification with microarray data, *Int. J. Neural Syst.* **15**(6) (2005) 475–484.
10. D. Chyzhyk and M. Graña, Discrimination of resting-state fMRI for schizophrenia patients with lattice computing based features, in *HAIS 2013*, eds. J.-S. Pan *et al.*, LNAI, Vol. 8073 (Springer, 2013), pp. 482–490.
11. M. Clos, K. Diederen, A. Meijering, I. Sommer and S. Eickhoff, Aberrant connectivity of areas for decoding degraded speech in patients with auditory verbal hallucinations, *Brain Struct. Funct.* **219**(2) (2014) 581–594.

12. J. Cutting, *The Right Cerebral Hemisphere and Psychiatric Disorders* (Oxford University Press, 1990).
13. S. Da Costa, W. van der Zwaag, J. Marques, R. Frackowiak, S. Clarke and M. Saenz, Human primary auditory cortex follows the shape of heschl's gyrus, *J Neurosci.* **31** (2011) 14067–14075.
14. A. D. de Weijer, S. F. Neggers, K. M. Diederen, R. C. Mandl, R. S. Kahn, H. E. Hulshoff Pol and I. E. Sommer, Aberrations in the arcuate fasciculus are associated with auditory verbal hallucinations in psychotic and in non-psychotic individuals, *Hum. Brain Mapp.* **34**(3) (2013) 626–634.
15. K. Diederen, S. Neggers, K. Daalman, J. Blom, R. Goekoop, R. Kahn and I. Sommer, Deactivation of the parahippocampal gyrus preceding auditory hallucinations in schizophrenia, *Am. J. Psychiatry* **167** (2010) 427–435.
16. T. Dierks, D. E. Linden, M. Jandl, E. Formisano, R. Goebel, H. Lanfermann and W. Singer, Activation of heschl's gyrus during auditory hallucinations, *Neuron* **22**(3) (1999) 615–621.
17. T. Ditman and G. Kuperberg, A source-monitoring account of auditory verbal hallucinations in patients with schizophrenia, *Harv. Rev. Psychiatry* **13** (2005) 280–299.
18. G. Dodgson and S. Gordon, Avoiding false negatives: Are some auditory hallucinations an evolved design flaw? *Behav. Cogn. Psychother.* **37** (2009) 325–334.
19. N. U. F. Dosenbach *et al.*, Prediction of individual brain maturity using fMRI, *Science* **329** (2010) 1358–1361.
20. I. Feinberg, Efference copy and corollary discharge: Implications for thinking and its disorders, *Schizophr. Bull.* **4**(4) (1978) 636–640.
21. I. Feinberg, Corollary discharge, hallucinations and dreaming, *Schizophr. Bull.* **37** (2011) 1–3.
22. G. M. W. J. First MB and Spitzer RL, *Structured Clinical Interview for DSM-IV-TR Axis I Disorders, Research Version, Patient Edition* (*SCID-I/P*) (Biometrics Research, New York State Psychiatric Institute, New York, NY, 2002).
23. J. Ford and D. Mathalon, Electrophysiological evidence of corollary discharge dysfunction in schizophrenia during talking and thinking, *J. Psychiatr. Res.* **38** (Jan 2004) 37–46.
24. K. J. Friston, Functional and effective connectivity in neuroimaging: A synthesis, *Hum. Brain Mapp.* **2** (1994) 56–78.
25. M. Gavrilescu, S. Rossell, G. W. Stuart, T. L. Shea, H. Innes-Brown, K. Henshall, C. McKay, A. A. Sergejew, D. Copolov and G. F. Egan, Reduced connectivity of the auditory cortex in patients with auditory hallucinations: A resting state functional magnetic resonance imaging study, *Psychol. Med.* **40**(7) (2010) 1149–1158.
26. D. Glotsos, J. Tohka, P. Ravazoula, D. Cavouras and G. Nikiforidis, Automated diagnosis of brain tumours astrocytomas using probabilistic neural network clustering and support vector machines, *Int. J. Neural Syst.* **15**(1) (2005) 1–11.
27. M. Graña, Lattice computing in hybrid intelligent systems, in *Proc. of the 2012 12th Int. Conf. on HIS* (*Hybrid Intelligent Systems*), ed. IEEE Press (4–7 December 2012), pp. 1–5.
28. M. Graña and D. Chyzhyk, Hybrid multivariate morphology using lattice auto-associative memories for resting-state fmri network discovery, *2012 12th Int. Conf. Hybrid Intelligent Systems* (*HIS*) (IEEE, 2012), pp. 537–542.
29. M. Graña, I. Villaverde, J. Maldonado and C. Hernández, Two lattice computing approaches for the unsupervised segmentation of hyperspectral images, *Neurocomputing* **72** (2009) 2111–2120.
30. M. Graña, D. Chyzhyk, M. Garcia-Sebastian and C. Hernandez, Lattice independent component analysis for functional magnetic resonance imaging, *Inform. Sci.* **181** (2011) 1910–1928.
31. M. D. Greicius, B. H. Flores, V. Menon, G. H. Glover, H. B. Solvason, H. Kenna, A. L. Reiss and A. F. Schatzberg, Resting-state functional connectivity in major depression: Abnormally increased contributions from subgenual cingulate cortex and thalamus, *Biol. Psychiatry* **62**(5) (2007) 429–437.
32. T. N. F. E. Haddock G and McCarron J, Scales to measure dimensions of hallucinations and delusions: The psychotic symptom rating scales (psyrats), *Psychol. Med.* **29**(4) (1999) 879–889.
33. M. Hauf, R. Wiest, K. Schindler, K. Jann, T. Dierks, W. Strik, G. Schroth and D. Hubl, Common mechanisms of auditory hallucinations — perfusion studies in epilepsy, *Psychiatry Res.: Neuroimaging* **211**(3) (2013) 268–270.
34. R. E. Hoffman, T. Fernandez, B. Pittman and M. Hampson, Elevated functional connectivity along a corticostriatal loop and the mechanism of auditory/verbal hallucinations in patients with schizophrenia, *Biol. Psychiatry* **69** (2011) 407–414.
35. R. Hoffman, A. Anderson, M. Varanko, J. Gore and M. Hampson, Time course of regional brain activation associated with onset of auditory/verbal hallucinations, *Br. J. Psychiatry* **193** (2008) 424–425.
36. K. Hugdahl, "Hearing voices": Auditory hallucinations as failure of top-down control of bottom-up perceptual processes, *Scand. J. Psychol.* **50**(6) (2009) 553–560.
37. T. Insel, B. Cuthbert, M. Garvey, R. Heinssen, D. Pine, K. Quinn, C. Sanislow and P. Wang, Research domain criteria (rdoc): Toward a new classification framework for research on mental disorders, *Am. J. Psychiatry* **167** (2010) 748–751.

38. T. Insel, The nimh research domain criteria (rdoc) project: Precision medicine for psychiatry, *Am. J. Psychiatry* **171** (2014) 395–397.
39. K. Jackowski, B. Krawcyk and M. Wozniak, Improved adaptive splitting and selection: The hybrid training method of a classifier based on a feature space partitioning, *Int. J. Neural Syst.* **24**(3) (2014) 1430007.
40. R. Jardri, A. Pouchet, D. Pins and P. Thomas, Cortical activations during auditory verbal hallucinations in schizophrenia: A coordinate-based meta-analysis, *Am. J. Psychiatry* **168** (2011) 73–81.
41. M. Johnson, S. Hastroudi and D. Lindsay, Source monitoring, *Psychol. Bull.* **114** (1993) 3–28.
42. S. Jones and C. Fernyhough, Neural correlates of inner speech and auditory verbal hallucinations: A critical review and theoretical integration, *Clin. Psychol. Rev.* **27**(2) (2007) 140–154.
43. V. Jumutc, P. Zayakin and A. Borisov, Ranking-based kernels in applied biomedical diagnostics using a support vector machine, *Int. J. Neural Syst.* **21**(6) (2011) 459–473.
44. V. Kaburlasos and A. Kehagias, Fuzzy inference system (fis) extensions based on the lattice theory, *IEEE Trans. Fuzzy Syst.* **22** (2014) 531–546.
45. V. Kaburlasos, S. Papadakis and G. Papakostas, Lattice computing extension of the fam neural classifier for human facial expression recognition, *IEEE Trans. Neural Netw. Learn. Syst.* **24** (2013) 1526–1538.
46. T. L. S. M. Kendall and J. D. Gibbons, *Rank Correlation Methods*, 5 edn. (Oxford University Press, USA, 1990).
47. T. Kohonen, *Associative Memory: A System-Theoretic Approach* (Springer, 1977).
48. K. M. Kubera, F. Sambataro, N. Vasic, N. D. Wolf, K. Frasch, D. Hirjak, P. A. Thomann and R. C. Wolf, Source-based morphometry of gray matter volume in patients with schizophrenia who have persistent auditory verbal hallucinations, *Prog. Neuro-Psychopharmacol. Biol. Psychiatry* **50** (2014) 102–109.
49. S. Kuhn and J. Gallinat, Quantitative meta-analysis on state and trait aspects of auditory verbal hallucinations in schizophrenia, *Schizophr. Bull.* **38** (2010) 779–786.
50. S. Lemm, B. Blankertz, T. Dickhaus and K.-R. Muller, Introduction to machine learning for brain imaging, *Neuroimage* **56**(2) (2011) 387–399.
51. B. R. Lennox, S. Bert, G. Park, P. B. Jones and P. G. Morris, Spatial and temporal mapping of neural activity associated with auditory hallucinations, *The Lancet* **353**(9153) (1999) 644.
52. B. R. Lennox, S. G. Park, I. Medley, P. G. Morris and P. B. Jones, The functional anatomy of auditory hallucinations in schizophrenia, *Psychiatry Res. Neuroimaging* **100**(1) (2000) 13–20.
53. D. Li, L. Xu, Goodman, Y. E. Xu and Y. Wu, Integrating a statistical background-foreground extraction algorithm and svm classifier for pedestrian detection and tracking, *Integr. Comput. Aided Eng.* **20**(3) (2013) 201–216.
54. E. J. Liemburg, A. Vercammen, G. J. Ter Horst, B. Curcic-Blake, H. Knegtering and A. Aleman, Abnormal connectivity between attentional, language and auditory networks in schizophrenia, *Schizophr. Res.* **135** (2012) 15–22.
55. Y. Liu, K. Wang, C. Yu, Y. He, Y. Zhou, M. Liang, L. Wang and T. Jiang, Regional homogeneity, functional connectivity and imaging markers of alzheimer's disease: A review of resting-state fmri studies, *Neuropsychologia* **46**(6) (2008) 1648–1656.
56. E. Lopez-Rubio, E.-J. Palomo and E. Dominguez, Bregman divergences for growing hierarchical self-organizing networks, *Int. J. Neural Syst.* **24**(4) (2014) 1450016.
57. H. Luo and S. Puthusserypady, Spatio-temporal modeling and analysis of fmri data using narx neural network, *Int. J. Neural Syst.* **16**(2) (2006) 139–149.
58. C. McKay, D. Headlam and D. Copolov, Central auditory processing in patients with auditory hallucinations, *Am. J Psychiatry* **157** (2000) 759–766.
59. A. Mechelli, P. Allen, E. Amaro, C. H. Fu, S. C. Williams, M. J. Brammer, L. C. Johns and P. K. McGuire, Misattribution of speech and impaired connectivity in patients with auditory verbal hallucinations, *Hum. Brain Mapp.* **28**(11) (2007) 1213–1222.
60. A. Meyer-Base, O. Lange, A. Wismuller and H. Ritter, Model-free functional mri analysis using topographic independent component analysis, *Int. J. Neural Syst.* **14**(4) (2004) 217–228.
61. G. Mingoia, G. Wagner, K. Langbein, S. Scherpiet, R. Schloesser, C. Gaser, H. Sauer and I. Nenadic, Altered default-mode network activity in schizophrenia: A resting state fmri study, *Schizophr. Res.* **117**(2–3) (2010) 355–356.
62. G. Modinos, S. Costafreda, M. van Tol, P. McGuire, A. Aleman and P. Allen, Neuroanatomy of auditory verbal hallucinations in schizophrenia: A quantitative meta-analysis of voxel-based morphometry studies, *Cortex* **49** (2013) 1046–1055.
63. J. Nazimek, M. Hunter and P. Woodruff, Auditory hallucinations: Expectation-perception model, *Med. Hypotheses* **78**(6) (2012) 802–810.
64. G. Northoff, N. W. Duncan and D. J. Hayes, The brain and its resting state activity–experimental and methodological implications, *Prog. Neurobiol.* **92**(4) (2010) 593–600.
65. G. Northoff and P. Qin, How can the brain's resting state activity generate hallucinations? A 'resting state hypothesis' of auditory verbal hallucinations, *Schizophr. Res.* **127**(1–3) (2011) 202–214.

66. S. Ocklenburg, R. Westerhausen, M. Hirnstein and K. Hugdahl, Auditory hallucinations and reduced language lateralization in schizophrenia: A meta-analysis of dichotic listening studies, *J. Int. Neuropsychol. Soc.* **19** (2013) 410–418.
67. V. Oertel, C. Knöchel, A. Rotarska-Jagiela, R. Schönmeyer, M. Lindner, V. van de Ven, C. Haenschel, P. Uhlhaas, K. Maurer and D. Linden, Reduced laterality as a trait marker of schizophrenia–Evidence from structural and functional neuroimaging, *J. Neurosci.* **30** (2010) 2289–2299.
68. V. Oertel-Knöchel, C. Knöchel, S. Matura, D. Prvulovic, D. E. J. Linden and V. van de Ven, Reduced functional connectivity and asymmetry of the planum temporale in patients with schizophrenia and first-degree relatives, *Schizophr. Res.* **147** (2013) 331–338.
69. L. Olson and M. Perry, Localization of epileptic foci using multimodality neuroimaging, *Int. J. Neural Syst.* **23**(1) (2013) 1230001.
70. D. Öngür, M. Lundy, I. Greenhouse, A. K. Shinn, V. Menon, B. M. Cohen and P. F. Renshaw, Default mode network abnormalities in bipolar disorder and schizophrenia, *Psychiatry Res. Neuroimaging* **183**(1) (2010) 59–68.
71. L. Palaniyappan, V. Balain, J. Radua and P. F. Liddle, Structural correlates of auditory hallucinations in schizophrenia: A meta-analysis, *Schizophr. Res.* **137**(1–3) (2012) 169–173.
72. F. Pereira, T. Mitchell and M. Botvinick, Machine learning classifiers and fMRI: A tutorial overview, *NeuroImage* **45**(1, Suppl 1) (2009) S199–S209.
73. P. Piaggi, D. Menicucci, C. Gentili, G. Handjaras, A. Gemignani and A. Landi, Adaptive filtering and random variables coefficient for analyzing functional magnetic resonance imaging data, *Int. J. Neural Syst.* **23**(3) (2013) 1350011.
74. P. Piaggi, D. Menicucci, C. Gentili, G. Handjaras, A. Gemignani and A. Landi, Singular spectrum analysis and adaptive filtering enhance the functional connectivity analysis of resting state fmri data, *Int. J. Neural Syst.* **24**(3) (2014) 1450010.
75. B. Raducanu, M. Grana and F. X. Albizuri, Morphological scale spaces and associative morphological memories: Results on robustness and practical applications, *J. Math. Imag. Vis.* **19**(2) (2003) 113–131.
76. D. Rangaprakash, X. Hu and G. Deshpande, Phase synchronization in brain networks derived from correlation between probabilities of recurrences in functional mri data, *Int. J. Neural Syst.* **23**(2) (2013) 1350003.
77. G. X. Ritter, P. Sussner and J. L. Diaz-de-Leon, Morphological associative memories, *IEEE Trans. Neural Netw.* **9**(2) (1998) 281–293.
78. G. Ritter, P. Gader and P. Hawkes, *Fixed Points of Lattice Transforms and Lattice Associative Memories*, Vol. 144 (Elsevier, 2006), pp. 165–242.
79. G. Ritter, J. Diaz-de-Leon and P. Sussner, Morphological bidirectional associative memories, *Neural Netw.* **12** (1999) 851–867.
80. A. Rotarska-Jagiela, V. van de Ven, V. Oertel-Knöchel, P. J. Uhlhaas, K. Vogeley and D. E. Linden, Resting-state functional network correlates of psychotic symptoms in schizophrenia, *Schizophr. Res.* **117**(1) (2010) 21–30.
81. A. K. Shinn, J. T. Baker, B. M. Cohen and D. Ongur, Functional connectivity of left heschl's gyrus in vulnerability to auditory hallucinations in schizophrenia, *Schizophr. Res.* **143**(2–3) (2013) 260–268.
82. N. Siddique and H. Adeli, *Computational Intelligence — Synergies of Fuzzy Logic, Neural Networks and Evolutionary Computing* (Wiley, West Sussex, United Kingdom, 2013).
83. I. E. Sommer, J. P. Selten, K. M. Diederen and J. D. Blom, Dissecting auditory verbal hallucinations into two components: Audibility (gedankenlautwerden) and alienation (thought insertion), *Psychopathology* **43**(2) (2010) 137–140.
84. I. E. Sommer, M. Clos, A. L. Meijering, K. M. J. Diederen and S. B. Eickhoff, Resting state functional connectivity in patients with chronic hallucinations, *PLoS ONE* **7**(9) (2012) e43516.
85. I. E. Sommer, K. Daalman, T. Rietkerk, K. M. Diederen, S. Bakker, J. Wijkstra and M. P. M. Boks, Healthy individuals with auditory verbal hallucinations; who are they? Psychiatric assessments of a selected sample of 103 subjects, *Schizophr. Bull.* **36**(3) (2010) 633–641.
86. R. Srikanth and A. G. Ramakrishnan, Wavelet-based estimation of hemodynamic response function from fmri data, *Int. J. Neural Syst.* **16**(2) (2006) 125–138.
87. P. Sussner and M. E. Valle, Gray-scale morphological associative memories, *IEEE Trans. Neural Netw.* **17** (2006) 559–570.
88. L. Tian and A. Noore, A novel approach for short-term load forecasting using support vector machines, *Int. J. Neural Syst.* **14**(5) (2004) 329–335.
89. A. Tien, Distributions of hallucinations in the population, *Soc. Psychiatry Psychiatr. Epidemiol.* **26**(6) (1991) 287–292.
90. V. Vapnik, *Statistical Learning Theory* (Wiley-Interscience, 1998).
91. F. Varese and R. Bentall, The metacognitive beliefs account of hallucinatory experiences: A literature review and meta-analysis, *Clin. Psychol. Rev.* **31** (2011) 850–864.
92. A. Vercammen, H. Knegtering, J. den Boer, E. J. Liemburg and A. Aleman, Auditory hallucinations

in schizophrenia are associated with reduced functional connectivity of the temporo-parietal area, *Biol. Psychiatry* **67**(10) (2010) 912–918.
93. L. Wang, P. Metzak and T. Woodward, Aberrant connectivity during self-other source monitoring in schizophrenia, *Schizophr. Res.* **125** (2011) 136–142.
94. F. Waters, J. Badcock, P. Michie and M. Maybery, Auditory hallucinations in schizophrenia: Intrusive thoughts and forgotten memories, *Cogn. Neuropsychiatry* **11** (2006) 65–83.
95. F. Waters, P. Allen, A. Aleman, C. Fernyhough, T. S. Woodward, J. C. Badcock, E. Barkus, L. Johns, F. Varese, M. Menon, A. Vercammen and F. Larøi, Auditory hallucinations in schizophrenia and nonschizophrenia populations: A review and integrated model of cognitive mechanisms, *Schizophr. Bull.* **38**(4) (2012) 683–693.
96. S. Whitfield-Gabrieli, H. W. Thermenos, S. Milanovic, M. T. Tsuang, S. V. Faraone, R. W. McCarley, M. E. Shenton, A. I. Green, A. Nieto-Castanon, P. LaViolette, J. Wojcik, J. D. E. Gabrieli and L. J. Seidman, Hyperactivity and hyperconnectivity of the default network in schizophrenia and in first-degree relatives of persons with schizophrenia, *Proc. Natl. Acad. Sci. U.S.A.* **106**(4) (2009) 1279–1284.
97. N. D. Wolf, F. Sambataro, N. Vasic, K. Frasch, M. Schmid, C. Schönfeldt-Lecuona, P. A. Thomann and R. C. Wolf, Dysconnectivity of multiple resting-state networks in patients with schizophrenia who have persistent auditory verbal hallucinations, *J Psychiatry Neurosci.* **36**(6) (2011) 366–374.
98. T. Yamanishi, J.-Q. Liu and H. Nishimura, Modeling fluctuations in default-mode brain network using a spiking neural network, *Int. J. Neural Syst.* **22**(4) (2012) 1250016.
99. Y. Yang and B.-L. Lu, Protein subcellular multi-localization prediction using a min-max modular support vector machine, *Int. J. Neural Syst.* **20**(1) (2010) 13–28.
100. Z. Yao, L. Wang, Q. Lu, H. Liu and G. Teng, Regional homogeneity in depression and its relationship with separate depressive symptom clusters: A resting-state fmri study, *J. Affec. Disord.* **115**(3) (2009) 430–438.
101. B. T. T. Yeo, F. M. Krienen, J. Sepulcre, M. R. Sabuncu, D. Lashkari, M. Hollinshead, J. L. Roffman, J. W. Smoller, L. Zöllei, J. R. Polimeni, B. Fischl, H. Liu and R. L. Buckner, The organization of the human cerebral cortex estimated by intrinsic functional connectivity, *J. Neurophysiol.* **106** (2011) 1125–1165.
102. Q. Yuan, W. Zhou, S. Yuan, X. Li, J. Wang and G. Jia, Epileptic EEg classification based on kernel sparse representation, *Int. J. Neural Syst.* **24**(4) (2014) 1450015.
103. Y.-F. Zang, Y. He, C.-Z. Zhu, Q.-J. Cao, M.-Q. Sui, M. Liang, L.-X. Tian, T.-Z. Jiang and Y.-F. Wang, Altered baseline brain activity in children with ADHD revealed by resting-state functional MRI, *Brain & Dev.* **29** (2007) 83–91.
104. Y. Zang, T. Jiang, Y. Lu, Y. He and L. Tian, Regional homogeneity approach to fMRI data analysis, *Neuroimage* **22** (2004) 394–400.
105. Y. Zhou, M. Liang, T. Jiang, L. Tian, Y. Liu, Z. Liu, H. Liu and F. Kuang, Functional dysconnectivity of the dorsolateral prefrontal cortex in first-episode schizophrenia using resting-state fmri, *Neurosci. Lett.* **417**(3) (2007) 297–302.
106. Y. Zhou, N. Shu, Y. Liu, M. Song, Y. Hao, H. Liu, C. Yu, Z. Liu and T. Jiang, Altered resting-state functional connectivity and anatomical connectivity of hippocampus in schizophrenia, *Schizophrenia Research* **100**(1–3) (2008) 120–132.
107. Q.-H. Zou, C.-Z. Zhu, Y. Yang, X.-N. Zuo, X.-Y. Long, Q.-J. Cao, Y.-F. Wang and Y.-F. Zang, An improved approach to detection of amplitude of low-frequency fluctuation (alff) for resting-state fmri: Fractional alff, *J. Neurosci. Methods* **172**(1) (2008) 137–141.
108. X.-N. Zuo, A. Di Martino, C. Kelly, Z. E. Shehzad, D. G. Gee, D. F. Klein, F. X. Castellanos, B. B. Biswal and M. P. Milham, The oscillating brain: Complex and reliable, *Neuroimage* **49** (2010) 1432–1445.